

# Quadratic speedups of multi-step probabilistic algorithms in state preparation

Hirofumi Nishi,<sup>1, 2, \*</sup> Taichi Kosugi,<sup>1, 2</sup> Yusuke Nishiya,<sup>1, 2</sup> and Yu-ichiro Matsushita<sup>1, 2, 3</sup>

<sup>1</sup>*Laboratory for Materials and Structures, Institute of Innovative Research,  
Tokyo Institute of Technology, Yokohama 226-8503, Japan*

<sup>2</sup>*Quemix Inc., Taiyo Life Nihombashi Building, 2-11-2, Nihombashi Chuo-ku, Tokyo 103-0027, Japan*

<sup>3</sup>*Quantum Material and Applications Research Center,  
National Institutes for Quantum Science and Technology,  
2-12-1, Ookayama, Meguro-ku, Tokyo 152-8552, Japan*

(Dated: August 8, 2023)

Quantum state preparation is a fundamental building block for various problems on a quantum computer. A non-unitary operator for that is designed to decay unwanted states contained in an initial state by introducing ancilla qubits, and it acts probabilistically on the initial state. In this study, we clarified that this probabilistic nature is a drag for quantum advantages: the probabilistic algorithms do not accelerate the computational speed over the classical ones. Combining quantum amplitude amplification (QAA) with multi-step probabilistic algorithms is proposed to address this drawback, leading to quadratic speedup and quantum advantages. We have also found that by the multi-step probabilistic method with QAA shows advantages than quantum phase estimation at the viewpoint of infidelity. We also demonstrated it to confirm the quadratic speedup, using a probabilistic imaginary-time evolution (PITE) method as an example.

*Introduction.* — Accurate and efficient calculation of ground states is greatly of importance in the field of quantum physics because it provides key insights into the properties and behavior of diverse quantum systems. Quantum phase estimation (QPE) [1–4], which is one of the promising quantum algorithms, offers an more efficient estimation of the eigenvalue for an input eigenvector of the Hamiltonian compared with a classical computer. Although the advantages of QPE have been known, the preparation of the input state for the QPE that should be as closer as possible to the ground state remains a problem. If the input state for the QPE contains only a small portion of the ground state, the probability for obtaining the ground-state energy decreases, as shown by scaling  $\mathcal{O}(|c_1|^2)$ , where  $|c_1|^2$  is the weight of the ground state in the input state. Thus, research into quantum algorithms for ground-state preparation has been actively pursued [5–18].

Some state preparation schemes utilizing non-unitary operations are proposed for obtaining the ground state [12–18]. Previous studies have realized an imaginary-time evolution (ITE) operator [13, 14, 17, 18], cosine functions [12, 15], and shifted step functions [10, 11] on quantum computers by introducing ancilla qubits and probabilistic nature, all schemes of which rely on forward- and backward-controlled real-time evolution (CRTE) operators. The implementation of real-time evolution (RTE) operators on a quantum computer has been well established in the context of Hamiltonian simulations based on Trotter decomposition [19–23], Taylor series [24, 25], and qubitization [26–29]. Thus, any sophisticated implementations of the RTE operators can be incorporated into the state-preparation schemes using non-unitary quantum circuits.

The computational costs of quantum algorithms for the probabilistic implementation of non-unitary operators were also investigated for the cosine function [9, 12, 15] and ITE operators [30]. These quantum algorithms incur the  $\mathcal{O}(|c_1|^{-2})$  computational cost to obtain the ground state. Especially, if  $|c_1| = 1/\sqrt{N}$ , where  $N = 2^n$  with  $n$  being the number of qubits, which corresponds to the situation that we don't know even the approximate ground state at all, at least  $\mathcal{O}(N)$  computational cost is required, which implies that quantum acceleration is not realized. Indeed, ground-state preparation is classified as complexity-class quantum Merlin-Arthur [31–33]. In this work, we propose a multi-step quantum algorithm showing quadratic speedup of the probabilistic state preparation scheme. The proposed quantum algorithm utilizes quantum amplitude amplification (QAA), which enhances the probability of obtaining the desired state through repeated operations. First, we summarize quantum algorithms for a probabilistic formalisms to implement non-unitary operators and its computational costs, in which we stress the computational scaling as  $\mathcal{O}(|c_1|^{-2})$  in probabilistic algorithms for state preparation, hindering the quantum advantages. We then show quantum algorithms for realizing quadratic speedup.

*Ground-state preparation.* — Now, let us consider a non-unitary operator  $f(\mathcal{H})$  where  $\mathcal{H}$  is the  $n$ -qubit system Hamiltonian. The non-unitary operator  $f(\mathcal{H})$  is embedded in the extended unitary matrix by introducing an ancilla qubit as

$$\mathcal{U} \equiv \begin{pmatrix} f(\mathcal{H}) & \sqrt{1 - f^2(\mathcal{H})} \\ \sqrt{1 - f^2(\mathcal{H})} & -f(\mathcal{H}) \end{pmatrix}, \quad (1)$$

consisting of the submatrices coupled to the ancillary  $|0\rangle$  and  $|1\rangle$  states. The desired state will be obtained when the ancilla is observed to be  $|0\rangle$ , while the state coupled to  $|1\rangle$  is undesired. Specifically, the action of the unitary

\* nishi.h.ac@m.titech.ac.jp

matrix  $\mathcal{U}$  on the input state leads to

$$f(\mathcal{H})|\psi\rangle \otimes |0\rangle + \sqrt{1 - f^2(\mathcal{H})}|\psi\rangle \otimes |1\rangle. \quad (2)$$

Any unitary matrix  $\mathcal{U}$  can be decomposed at least first order of  $\mathcal{H}$  (See the details in Supplementary Materials (SM) [34]), and implemented using forward- and backward-CRTE operations and single-qubit gates as shown in Fig. 1.

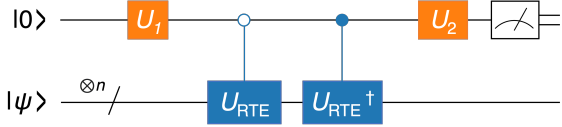


FIG. 1. Quantum circuit of probabilistic algorithm for ground state preparation. The circuit is composed of a single ancilla qubit and forward- and backward-CRTE gates.

In operating  $\mathcal{U}$  repeatedly, the unitary matrix  $\mathcal{U}$  contains some parameters, such as real time-step size  $\Delta\tau$  in Fig. 1, which can be chosen freely at each step. The unitary  $\mathcal{U}$  at the  $k$ th step is denoted by  $\mathcal{U}_k$  to specify the step dependence. When we use  $K$  ancilla qubits and use a different ancilla qubit for each  $\mathcal{U}_k$  without measuring the ancilla qubits, the actions of  $\{\mathcal{U}_k\}$  on the input state with the initialized ancilla qubits lead to

$$F_K(\mathcal{H})|\psi\rangle \otimes |0\rangle^{\otimes K} + (\text{other states}). \quad (3)$$

where  $F_K(\mathcal{H}) \equiv \prod_{k=1}^K f_k(\mathcal{H})$ . Note that the use of only one ancilla qubit is allowed if we reuse the ancilla qubit from the previous step after measuring and initializing it. References [14] and [12] implemented  $f_k(\mathcal{H})$  as an approximate ITE operator  $e^{-\Delta\tau_k \mathcal{H}}$  and cosine function  $\cos(t_k \mathcal{H})$ , respectively. Specific quantum circuits are summarized in SM [34]. The repeated operations of  $f_k(\mathcal{H})$  result in decaying unwanted states, such as excited states. Quantum signal processing is another approach for designing such decay functions [27], in which the shifted step function is approximated with a Chebyshev polynomial and implemented with a single ancilla qubit [10, 11].

Observing all the ancilla qubits as  $|0\rangle$  state leads to collapse from the entangled wave function to

$$|\Psi_K\rangle = \frac{1}{\sqrt{P_K}} F_K(\mathcal{H})|\psi\rangle, \quad (4)$$

where  $P_K$  is the total success probability of all steps being successful. The input state is expanded as  $|\psi\rangle = \sum_{i=1}^N c_i |\lambda_i\rangle$ , where  $|\lambda_i\rangle$  is the  $i$ th eigenstate of the Hamiltonian  $\mathcal{H}$  and  $c_i$  is the expansion coefficient. For simplicity, in this study, we assume non-degenerate and ascending order of the eigenvalues, but generalization is straightforward. If  $F_K(\mathcal{H})$  is well designed to decay unwanted state, then the total success probability goes to

$$P_K = \frac{1}{1 - \delta_K} |c_1|^2, \quad (5)$$

where  $\delta_K$  is the infidelity defined as  $\delta_K \equiv 1 - \mathcal{F}_K$  with the fidelity  $\mathcal{F}_K \equiv |\langle \lambda_1 | \Psi_K \rangle|^2$  (See the details in SM [34]). Here, we assume  $F_K(\lambda_1) = 1$ , which is realized by a constant energy shift in the PITE [30]. Every quantum algorithm that decays the unwanted state to achieve a small amount of  $\delta_K$  by a non-unitary operation shows the scaling of the total success probability as  $\mathcal{O}(|c_1|^2)$ . Importantly, this fact means that the scaling of the total success probability is irrelevant to the type of non-unitary operator  $f_k(\mathcal{H})$ , number of ancilla qubits, or circuit implementation method for  $f_k(\mathcal{H})$ . If we don't know even the approximate ground state at all, e.g.,  $|c_i|^2 = 1/N$  for each  $i$ , the computational cost of at least one success scales as  $\mathcal{O}(N)$ . No quantum acceleration was observed for these algorithms. On the other hand, the CRTE gates are efficiently implemented in polynomial cost [19–29]. For example, the circuit depth for CRTE for an  $n_e$ -electron system based on first quantization Hamiltonian scales as  $d_{\text{CRTE}} = \mathcal{O}(rn_e^2 \text{poly}(\log(n_e^{1/3}/\Delta x)))$ , where  $\Delta x$  represents the grid spacing of the discretized space and  $r$  is the Trotter number dividing imaginary-time step size [14, 21]. Then, the computational cost is

$$\frac{d_{\text{CRTE}K}}{P_K} = \mathcal{O}\left(\frac{d_{\text{CRTE}}}{|c_1|^2} \ln\left(\frac{(1 - \delta_K)(1 - |c_1|^2)}{\delta_K |c_1|^2}\right)\right), \quad (6)$$

(See the details in SM [34]).

*Quantum Amplitude Amplification.* — One possibility to realize the quantum acceleration with probabilistic algorithms for ground state preparation is to introduce a multi-step scheme and combine QAA with it [29, 35–37]. We consider a  $K$ -step probabilistic quantum circuit with  $K$  ancilla qubits. Each ancilla qubit corresponds to each step of the probabilistic algorithm, and the measurement of all the ancilla qubits is performed after the final step. The output state just before the measurement is of the form

$$|\tilde{\Psi}\rangle = a|\Psi_{\text{good}}\rangle + \sqrt{1 - a}|\Psi_{\text{bad}}\rangle, \quad (7)$$

where

$$|\Psi_{\text{good}}\rangle = \frac{1}{\sqrt{P_K}} F_K(\mathcal{H})|\psi\rangle \otimes |0\rangle^{\otimes K} \quad (8)$$

is the desired state having a weight  $a$  and  $|\Psi_{\text{bad}}\rangle$  is the orthogonal state to  $|\Psi_{\text{good}}\rangle$ . QAA enhances the coefficients of the  $|\Psi_{\text{good}}\rangle$  state by the  $m$  times action  $\prod_{i=1}^m Q(\phi_{2i-1}, \phi_{2i})$  of an amplitude amplification operator defined as

$$Q(\phi_{2i-1}, \phi_{2i}) \equiv -\mathcal{U}_{\text{REF}}^{(K)} S_0^{(n+K)}(\phi_{2i-1}) \left(\mathcal{U}_{\text{REF}}^{(K)}\right)^\dagger S_\chi(\phi_{2i}). \quad (9)$$

Here,  $S_\chi$  is an oracle,  $S_0$  is a zero reflection, and  $\mathcal{U}_{\text{REF}}^{(K)}$  is defined as  $\mathcal{U}_{\text{REF}}^{(K)}|0\rangle^{\otimes(n+K)} = |\tilde{\Psi}\rangle$ . The rotation angles  $\{\phi_i\}$  is chosen as  $\phi_i = \pm\pi$  in the conventional way [35, 36], but recently approaches have been proposed to

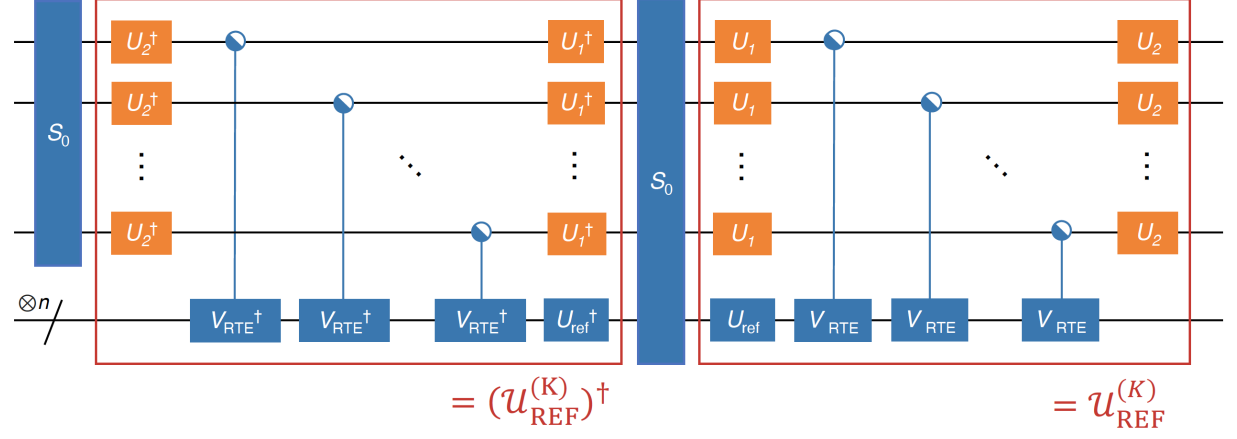


FIG. 2. The quantum circuit for the amplitude amplification operator of the probabilistic algorithm for ground-state preparation in Eq. (9) while ignoring the global phase. The forward and backward CRTE gates are combined and denoted as the controlled-V<sub>RTE</sub> gate.  $S_0$  on the left represents  $S_0^{(K)}(\phi_{2i})$ , while that on the right represents  $S_0^{(n+K)}(\phi_{2i-1})$ .  $U_{\text{ref}}$  is defined as  $U_{\text{ref}}|0\rangle^{\otimes n} \equiv |\psi\rangle$ , which is the input state before the PITE circuit. In the red box on the right,  $V_{\text{RTE}} = V_{\text{RTE}}(t_1)$ ,  $V_{\text{RTE}} = V_{\text{RTE}}(t_2), \dots, V_{\text{RTE}} = V_{\text{RTE}}(t_K)$  from the left, and  $U_1 = U_1^{(1)}, U_1 = U_1^{(2)}, \dots, U_1 = U_1^{(K)}$  from the top where  $U_1^{(k)}$  is  $U_1$  in the  $k$ th step. The same applies to  $U_2$ .

determine  $\{\phi_i\}$  so that the increase in success probability is an approximated sign function [29, 37]. The zero reflection and oracle rotate the output state  $|\tilde{\Psi}\rangle$  in the effective two-dimensional space spanned by  $|\Psi_{\text{good}}\rangle$  and  $|\Psi_{\text{bad}}\rangle$ , which are represented by  $S_0^{(n)}(\phi) = e^{i\phi|0\rangle\langle 0|^{\otimes n}}$  and  $S_\chi(\phi) = I_{2^n} \otimes S_0^{(K)}(\phi)$ , respectively. The circuit depth of the zero reflection scales as  $\mathcal{O}(n)$  with a single ancilla qubit [38], and Maslov's gate reduces the scaling preconstant [39]. Figure 2 shows the amplitude amplification operator  $Q$  for the probabilistic algorithm for state preparation in  $K$  steps.

The optimal number of repetitions of QAA is derived as

$$m^* = \left\lfloor \frac{(2n+1)\pi}{4\sin^{-1} a} \right\rfloor. \quad (10)$$

Thus, when the total success probability  $P_K$  is small, we execute a first-order Taylor expansion for  $\sin^{-1} a$  and obtain the order of optimal repetitions  $m^*$  as  $m^* = \mathcal{O}(1/|c_1|)$ . Accordingly, the computational cost for PITE combined with QAA (hereinafter referred to as multi-step PITE) is estimated as

$$d_{\text{CRTE}} K m^* = \mathcal{O} \left( \frac{d_{\text{CRTE}}}{|c_1|} \ln \left( \frac{(1 - \delta_K)(1 - |c_1|^2)}{\delta_K |c_1|^2} \right) \right), \quad (11)$$

where we see that the QAA technique achieves quadratic speedup from Eq. (6). We also discussed the technique of PITE combined with QAA in reference [40], where a short-depth circuit for first-step PITE and circuit construction for  $K$  steps using one ancilla qubit are proposed. This multi-step PITE that we propose in this work is a natural extension of the Ref. [40] and clearly show the quadratic acceleration for the whole process of the PITE.

*Quantum phase estimation* — QPE is a standard building block not only to estimate the ground state energy but also to prepare the ground state. Before comparing multi-step PITE with QPE in the numerical results, we briefly discuss QPE. QPE based on QFT achieves the Heisenberg scaling. Although QPE based on QFT requires many ancilla qubits, reusing an ancilla qubit after a measurement and operating subsequent operations depending on the observation enable us to perform the same estimation with one ancilla qubit [4, 41–43]. For simplicity, we used the standard QPE based on the QFT. After each run of QPE, one of the eigenenergies is loaded onto the ancilla qubits in a binary representation. We consider the situation where the input state for the QPE is  $|\psi\rangle = \sum_{i=1}^N c_i |\lambda_i\rangle$  and that  $K$  ancilla qubits are used. Note that through the QPE all eigenvalues,  $\{\lambda_i\}$ , where we assume ascending order, are expressed by binary representation  $\{k_i\}$ . In realistic situation that finite number of ancilla qubits are available, some different eigenvalues  $\{\lambda_i\}$  which are energetically close to each other and inside an energy resolution,  $1/T$ , can be mapped to the same binary representation  $k_i$ , where  $T \equiv 2^K$ . When we observe  $k$  as the binary representation of the estimated eigenvalue, the input state has collapsed to

$$|\Psi_{\text{QFT}}\rangle = \frac{1}{\sqrt{P_k}} \sum_{i=1}^N c_i \alpha_{k|i} |\lambda_i\rangle, \quad (12)$$

where the state is normalized with the probability  $P_k = \sum_{i=1}^N |c_i|^2 |\alpha_{k|i}|^2$  and periodic function  $\alpha_{k|i}$  is defined as  $\alpha_{k|i} \equiv (1/T) \sum_{\tau=0}^{T-1} e^{2\pi i \tau (\lambda_i t_0 - k)/T}$ . Here,  $t_0$  is a scaling parameter used to enlarge or shrink the eigenvalues for precise measurement. As clearly from  $T \equiv 2^K$ , the more ancilla qubits we use, the finer the resolution of the eigenvalue is; thus, we choose  $t_0 = 2^{K-N_C}$  where

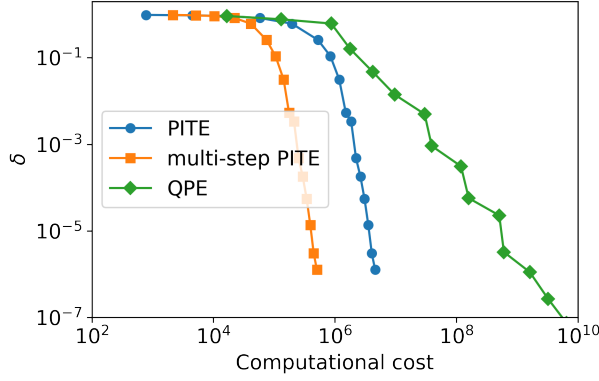


FIG. 3. Plots of infidelity  $\delta_K$  as a function of computational cost for PITE, multi-step PITE, and QPE, respectively. The results were obtained using the one-dimensional Heisenberg chain with eight spins.

$N_C = \lfloor \log_2(\lambda_N - \lambda_1) \rfloor$ . Because the number of queries to CRTE increases exponentially, the computational cost for QPE to obtain the ground state eigenvalue is given by  $\mathcal{O}(1/(\sqrt{\delta_K}|c_1|^2))$  [9, 34]. We stress that by comparing Eq. (6), PITE has an exponential advantage in terms of computational cost with respect to the infidelity  $\delta_K$  over QPE.

*Numerical results.* — Numerical simulation demonstrates the strengths of the proposed method, which was carried out using Qiskit, an open-source library for quantum simulation [44]. The Heisenberg model was adopted as the computational model:

$$\mathcal{H} = \sum_{\langle j,k \rangle} \vec{\sigma}_j \cdot \vec{\sigma}_k + \sum_j h_j \sigma_j^z \quad (13)$$

where  $\vec{\sigma}_j = (\sigma_j^x, \sigma_j^y, \sigma_j^z)$  is the Pauli matrix acting on the  $j$ th spin and  $\langle j, k \rangle$  represents the combination of the nearest neighbors of the closed one-dimensional chain.  $h_j$  represents the strength of the magnetic field, which was randomly chosen from a uniform distribution as  $h_j \in [-1, 1]$ . The CRTE gate is implemented by the fourth-order Trotter decomposition [45] for even-odd groups of the Hamiltonian [22, 23]. The dependence of the accuracy and total computational complexity on the order of Trotter decomposition is numerically presented in SM [34]. The multi-step PITE method was adopted as a probabilistic algorithm to prepare the ground state. The PITE method employs a constant energy shift to increase the total success probability, and adopts computationally efficient scheduling of the imaginary-time step size [30].

Figure 3 shows the infidelity  $\delta_K$  as a function of the computational costs for QPE, PITE, and multi-step PITE. The initial state is chosen as uniform probability weights with respect to each eigenvector, i.e.,  $|c_i|^2 = 1/N$ . As the number of steps in PITE or the number of digits, i.e., resolution in QPE increases, the infidelity decreases, while the computational cost increases. As the infidelity decreases, the success probability decreases and

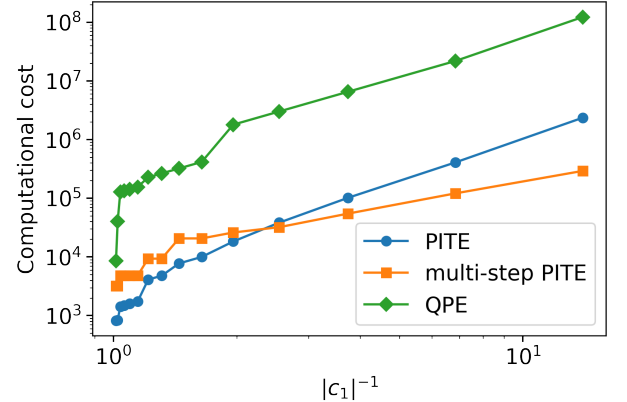


FIG. 4. Plots of computational cost for PITE, multi-step PITE, and QPE as a function of the inverse probability weight of the ground state in the input state.

approaches  $1/N$ . This behavior is common to PITE and QPE. The difference between PITE and QPE is the number of queries to the CRTE block. In QPE, the number of queries increases exponentially, and thus, the computational cost increases linearly with the infidelity. However, because the query of PITE increases linearly, the number of partitions for the imaginary-time step size is linear. The figure confirms that PITE is exponentially faster than QPE with respect to the infidelity  $\delta_K$ , as given by Eq. (6). Furthermore, for multi-step PITE, we observe an acceleration in the computational cost that may be due to the quadratic speedup with respect to the success probability, although there is an overhead due to zero-reflections. We verified the method with different orders and used the fourth-order Trotter, which is in good agreement with the exact solution [34].

To clearly observe the quadratic speedup with respect to the probability weight  $|c_1|^2$  of the ground state by multi-step PITE, the dependence of the computational cost on varying  $|c_1|^2$  is shown in Figure 4. The computational cost was estimated when the infidelity was below  $\delta_K = 10^{-4}$ . The probability weight of the initial state was determined from a Gaussian distribution as a function of the eigenvalues, with the mean of the ground state energy. The probability weight of the ground states is increased by changing the variance of the Gaussian distribution. The computational cost of PITE is lower than that of QPE for the entire region owing to the exponential advantage of PITE for the infidelity  $\delta_K$ . Although the computational cost of multi-step PITE becomes larger than that of PITE without QAA at  $|c_1| \approx 1/2$  because of the overhead of the QAA operation, it decreases as  $|c_1|^{-1}$  increases for  $|c_1| < 1/2$ . Accordingly, quadratic speedup by QAA was observed. The crossing point of the computational cost of PITE and multi-step PITE is determined by the relationship between the circuit depth of PITE and the zero reflection [34]. As the computational overhead of the zero reflection becomes smaller, QAA brings benefit for the computational cost over a

wide range.

*Conclusions.* — In this letter, we proposed a quantum algorithm for ground-state preparation that presents quantum advantages. The recently proposed PITE method, comprising a single ancilla qubit and forward- and backward-CRTE operations, non-variationally calculates the ground state on a quantum computer. Although PITE presents an exponential advantage over QPE for an infidelity  $\delta$ , its probabilistic nature worsens the computational cost to scale as  $\mathcal{O}(|c_1|^{-2} \log \delta^{-1})$ , where  $|c_1|^2$  is the probability weight of the ground state in the initial state. Here, combining QAA with PITE offers quadratic speedup over the classical one, where the delayed measurement succeeded in multistep amplitude amplification. The numerical simulations emphasized the strengths of the proposed algorithm. The proposed algorithm is assumed to be implemented on a fault-tolerant quantum computer (FTQC). However, the development of quantum algorithms for early FTQC or post-noisy

intermediate-scale quantum devices is an important research topic. Accordingly, reducing the ancilla qubits and circuit depth of this algorithm is a promising direction for future work. In addition, preparing a good initial state using classical pre-processing contributes to fast quantum state preparation, regardless of whether QAA is applied. By combining the proposed algorithm, various physical quantities such as the one-body Green's function [46] linear response function [47], and microcanonical and canonical properties [48] can be calculated. This method is also applicable to various problems, such as optimizing the structure geometry based on an exhaustive search [49] and an electron under a magnetic field [50]. Thus, this study will contribute to the numerical simulations of material science on quantum computers.

This work was supported by MEXT under "Program for Promoting Researches on the Supercomputer Fugaku" (JPMXP1020200205) and by JSPS KAKENHI under Grant-in-Aid for Scientific Research (A) No. 21H04553.

---

[1] A. Y. Kitaev, *Quantum measurements and the abelian stabilizer problem* (1995).

[2] D. S. Abrams and S. Lloyd, *Phys. Rev. Lett.* **83**, 5162 (1999).

[3] Z. Ding and L. Lin, Simultaneous estimation of multiple eigenvalues with short-depth quantum circuit on early fault-tolerant quantum computers (2023), [arXiv:2303.05714 \[quant-ph\]](https://arxiv.org/abs/2303.05714).

[4] Z. Ding and L. Lin, *PRX Quantum* **4**, 020331 (2023).

[5] T. Kadowaki and H. Nishimori, *Phys. Rev. E* **58**, 5355 (1998).

[6] E. Farhi, J. Goldstone, S. Gutmann, and M. Sipser, *Quantum computation by adiabatic evolution* (2000).

[7] A. Aspuru-Guzik, A. D. Dutoi, P. J. Love, and M. Head-Gordon, *Science* **309**, 1704 (2005), <https://www.science.org/doi/pdf/10.1126/science.1113479>.

[8] D. Poulin and P. Wocjan, *Phys. Rev. Lett.* **102**, 130503 (2009).

[9] Y. Ge, J. Tura, and J. I. Cirac, *Journal of Mathematical Physics* **60**, 022202 (2019).

[10] L. Lin and Y. Tong, *Quantum* **4**, 372 (2020).

[11] L. Lin and Y. Tong, *PRX Quantum* **3**, 010318 (2022).

[12] K. Choi, D. Lee, J. Bonitati, Z. Qian, and J. Watkins, *Phys. Rev. Lett.* **127**, 040505 (2021).

[13] T. d. L. Silva, M. M. Taddei, S. Carrazza, and L. Aolita, *Fragmented imaginary-time evolution for early-stage quantum signal processors* (2021).

[14] T. Kosugi, Y. Nishiya, H. Nishi, and Y.-i. Matsushita, *Phys. Rev. Research* **4**, 033121 (2022).

[15] R. Meister and S. C. Benjamin, *Resource-frugal hamiltonian eigenstate preparation via repeated quantum phase estimation measurements* (2022).

[16] I. Stetcu, A. Baroni, and J. Carlson, *Projection algorithm for state preparation on quantum computers* (2022).

[17] H.-N. Xie, S.-J. Wei, F. Yang, Z.-A. Wang, C.-T. Chen, H. Fan, and G.-L. Long, *A probabilistic imaginary time evolution algorithm based on non-unitary quantum circuit* (2022).

[18] H. H. S. Chan, D. Muñoz-Ramo, and N. Fitzpatrick, *Simulating non-unitary dynamics using quantum signal processing with unitary block encoding* (2023).

[19] S. Lloyd, *Science* **273**, 1073 (1996), <https://www.science.org/doi/pdf/10.1126/science.273.5278.1073>.

[20] D. S. Abrams and S. Lloyd, *Phys. Rev. Lett.* **79**, 2586 (1997).

[21] I. Kassal, S. P. Jordan, P. J. Love, M. Mohseni, and A. Aspuru-Guzik, *Proceedings of the National Academy of Sciences* **105**, 18681 (2008), <https://www.pnas.org/doi/pdf/10.1073/pnas.0808245105>.

[22] A. M. Childs and Y. Su, *Phys. Rev. Lett.* **123**, 050503 (2019).

[23] A. M. Childs, Y. Su, M. C. Tran, N. Wiebe, and S. Zhu, *Phys. Rev. X* **11**, 011020 (2021).

[24] A. M. Childs and N. Wiebe, *Quantum Info. Comput.* **12**, 901–924 (2012).

[25] D. W. Berry, A. M. Childs, R. Cleve, R. Kothari, and R. D. Somma, *Phys. Rev. Lett.* **114**, 090502 (2015).

[26] G. H. Low and I. L. Chuang, *Phys. Rev. Lett.* **118**, 010501 (2017).

[27] G. H. Low and I. L. Chuang, *Quantum* **3**, 163 (2019).

[28] A. Gilyén, Y. Su, G. H. Low, and N. Wiebe, in *Proceedings of the 51st Annual ACM SIGACT Symposium on Theory of Computing*, STOC 2019 (Association for Computing Machinery, New York, NY, USA, 2019) p. 193–204.

[29] J. M. Martyn, Z. M. Rossi, A. K. Tan, and I. L. Chuang, *PRX Quantum* **2**, 040203 (2021).

[30] H. Nishi, K. Hamada, Y. Nishiya, T. Kosugi, and Y. ichiro Matsushita, *Analyzing computational cost of probabilistic imaginary-time evolution method* (2023), [arXiv:2305.04600 \[quant-ph\]](https://arxiv.org/abs/2305.04600).

[31] A. Y. Kitaev, A. Shen, and M. N. Vyalyi, *Classical and quantum computation*, 47 (American Mathematical Soc., 2002).

[32] J. Kempe, A. Kitaev, and O. Regev, in *FSTTCS 2004: Foundations of Software Technology and Theoretical Computer Science*, edited by K. Lodaya and M. Mahajan (Springer Berlin Heidelberg, Berlin, Heidelberg, 2005) pp. 372–383.

[33] R. Oliveira and B. M. Terhal, The complexity of quantum spin systems on a two-dimensional square lattice (2008), [arXiv:quant-ph/0504050 \[quant-ph\]](https://arxiv.org/abs/quant-ph/0504050).

[34] See Supplementary Material.

[35] G. Brassard and P. Hoyer, in *Proceedings of the Fifth Israeli Symposium on Theory of Computing and Systems* (1997) pp. 12–23.

[36] G. Brassard, P. Hoyer, M. Mosca, and A. Tapp, arXiv e-prints , quant-ph/0005055 (2000), [arXiv:quant-ph/0005055 \[quant-ph\]](https://arxiv.org/abs/quant-ph/0005055).

[37] T. J. Yoder, G. H. Low, and I. L. Chuang, *Phys. Rev. Lett.* **113**, 210501 (2014).

[38] A. Barenco, C. H. Bennett, R. Cleve, D. P. DiVincenzo, N. Margolus, P. Shor, T. Sleator, J. A. Smolin, and H. Weinfurter, *Phys. Rev. A* **52**, 3457 (1995).

[39] D. Maslov, *Phys. Rev. A* **93**, 022311 (2016).

[40] H. Nishi, T. Kosugi, Y. Nishiya, and Y.-i. Matsushita, *Acceleration of probabilistic imaginary-time evolution method combined with quantum amplitude amplification* (2022).

[41] R. B. Griffiths and C.-S. Niu, *Phys. Rev. Lett.* **76**, 3228 (1996).

[42] B. L. Higgins, D. W. Berry, S. D. Bartlett, H. M. Wiseman, and G. J. Pryde, *Nature* **450**, 393 (2007).

[43] D. W. Berry, B. L. Higgins, S. D. Bartlett, M. W. Mitchell, G. J. Pryde, and H. M. Wiseman, *Phys. Rev.* **A** **80**, 052114 (2009).

[44] Qiskit contributors, *Qiskit: An open-source framework for quantum computing* (2023).

[45] M. Suzuki, *Journal of Mathematical Physics* **32**, 400 (1991).

[46] T. Kosugi and Y.-i. Matsushita, *Phys. Rev. A* **101**, 012330 (2020).

[47] T. Kosugi and Y.-i. Matsushita, *Phys. Rev. Research* **2**, 033043 (2020).

[48] S. Lu, M. C. Bañuls, and J. I. Cirac, *PRX Quantum* **2**, 020321 (2021).

[49] T. Kosugi, H. Nishi, and Y. Matsushita, *Exhaustive search for optimal molecular geometries using imaginary-time evolution on a quantum computer* (2022).

[50] T. Kosugi, H. Nishi, and Y. ichiro Matsushita, *Japanese Journal of Applied Physics* **62**, 062004 (2023).

[51] M. A. Nielsen, I. L. Chuang, I. L. Chuang, et al., *Quantum Computation and Quantum Information* (Cambridge University Press, 2000).

[52] R. R. Tucci, An introduction to cartan’s kak decomposition for qc programmers (2005), [arXiv:quant-ph/0507171 \[quant-ph\]](https://arxiv.org/abs/quant-ph/0507171).

[53] C. Developers, *Cirq* (2022), See full list of authors on Github: <https://github.com/quantumlib/Cirq/graphs/contributors>.

[54] P. Hohenberg and W. Kohn, *Phys. Rev.* **136**, B864 (1964).

[55] W. Kohn and L. J. Sham, *Phys. Rev.* **140**, A1133 (1965).

[56] R. J. Bartlett and M. Musial, *Rev. Mod. Phys.* **79**, 291 (2007).

[57] T. Helgaker, P. Jorgensen, and J. Olsen, *Molecular electronic-structure theory* (John Wiley & Sons, 2013).

---

## Supplementary Material: Quadratic speedups of multi-step probabilistic algorithms in state preparation

### S1. IMPLEMENTATION OF NON-UNITARY OPERATOR IN PROBABILISTIC WAY

#### A. Probabilistic imaginary-time evolution method

##### 1. Exact non-unitary operator

Our previous works [S14, S40] presented the quantum circuit for probabilistic operating the non-unitary Hermitian operator  $f(\mathcal{H})$ , where  $\mathcal{H}$  is the Hamiltonian of  $n$ -qubit system. The quantum circuits for the non-unitary operation  $f(\mathcal{H})$  are shown in Fig. S1(a), which is comprising of a single ancilla qubit and two controlled unitary gates  $e^{\pm\kappa\Theta}$ . The generators of the unitary gates is given by  $\pm\kappa\Theta$  where

$$\Theta \equiv \arccos \left[ \frac{f(\mathcal{H}) + \sqrt{1 - [f(\mathcal{H})]^2}}{\sqrt{2}} \right], \quad (\text{S1})$$

is a Hermitian operator for  $n$ -qubit system and

$$\kappa \equiv \text{sgn} \left( \|f(\mathcal{H})\| - \frac{1}{\sqrt{2}} \right), \quad (\text{S2})$$

is defined to lead to  $\cos\Theta = (f(\mathcal{H}) + \sqrt{1 - f^2(\mathcal{H})})$  and  $\sin\kappa\Theta = (f(\mathcal{H}) - \sqrt{1 - f^2(\mathcal{H})})$ . In addition, the single-qubit gate in Fig. S1(a) is defined as

$$W \equiv \frac{1}{\sqrt{2}} \begin{pmatrix} 1 & -i \\ 1 & i \end{pmatrix}. \quad (\text{S3})$$

An interesting non-unitary operator is the imaginary time evolution (ITE) operator, expressed as

$$f(\mathcal{H}) = \Gamma e^{-\tau \mathcal{H}}, \quad (\text{S4})$$

where  $\tau$  is the imaginary time.  $\Gamma$  is an adjustable parameter. The ITE operator successfully acts on the target qubits when the ancilla qubit is observed as  $|0\rangle$  state. In contrast, when the ancilla qubit is observed as  $|1\rangle$  state, the target qubits become an undesired state. Because the state acted on by the ITE operator is probabilistically obtained, this method is called the probabilistic imaginary-time evolution (PITE) method.

### 2. Approximate non-unitary operator

The implementation method for the unitary  $e^{\pm i\kappa\Theta}$  is not straightforward; thus, we approximate it as the first order of  $\mathcal{H}$ . To do this, we first decompose the non-unitary  $f(\mathcal{H})$  as a product consisting of  $K$  factors, so that the approximation is well constructed. The  $f(\mathcal{H})$  is rewritten as  $F_K(\mathcal{H})$  explicitly indicating the parameter  $K$  and each factor is denoted as  $f_k(\mathcal{H})$ :  $F_K(\mathcal{H}) = \prod_{k=1}^K f_k(\mathcal{H})$ . To distinguish the variables at different steps, we denote the variable at the  $k$ th step by the subscript  $k$ . Executing the first-order Trotter decomposition leads to

$$\kappa\Theta_k = a_0^{(k)} + a_1^{(k)}\mathcal{H} + \mathcal{O}(\mathcal{H}^2), \quad (\text{S5})$$

where  $a_0^{(k)}$  and  $a_1^{(k)}$  are coefficients of the Taylor expansion, which depend on the type of non-unitary  $f_k(\mathcal{H})$ .

Consider the ITE operator  $\Gamma e^{-\tau \mathcal{H}}$  as an example. First, the imaginary time  $\tau$  is divided into small fragments:  $\tau \equiv \sum_{k=1}^K \Delta\tau_k$ . The ITE operator for imaginary-time  $\tau$  is decomposed as

$$\Gamma e^{-\tau \mathcal{H}} = \prod_{k=1}^K \gamma_k e^{-\Delta\tau_k \mathcal{H}}, \quad (\text{S6})$$

where  $\Gamma = \prod_{k=1}^K \gamma_k$ .  $\gamma_k$  is an adjustable parameter that satisfies the conditions  $0 < \gamma < 1$  and  $\gamma \neq 1/\sqrt{2}$ , and is introduced to avoid singularity. The ITE operator for a small imaginary time  $\gamma_k e^{-\Delta\tau_k \mathcal{H}}$  was implemented in the manner described above. When the arccosine function in Eq. (S1) is intended for  $f_k(\mathcal{H}) = \gamma_k e^{-\Delta\tau_k \mathcal{H}}$ , the coefficients of the Taylor expansion is calculated as  $a_0^{(k)} \equiv \kappa \arccos \left[ (\gamma_k + \sqrt{1 - \gamma_k^2})/\sqrt{2} \right]$  and  $a_1^{(k)} \equiv \gamma_k / \sqrt{1 - \gamma_k^2}$ . Consequently, the approximated non-unitary operator in the first order of  $\Delta\tau_k$  is given by

$$\begin{aligned} f_k(\mathcal{H}) &= \gamma_k \left[ \cos(\mathcal{H}\Delta\tau_k s_k) - \frac{1}{s_k} \sin(\mathcal{H}\Delta\tau_k s_k) \right] \\ &= \sin(-\mathcal{H}\Delta\tau_k s_k + \varphi_k), \end{aligned} \quad (\text{S7})$$

where  $s_k = \tan \varphi_k$ .

The quantum circuit for the approximate PITE operator is illustrated in Fig. S1(b). This quantum circuit comprises forward- and backward-controlled real-time evolution (CRTE) operators. The CRTE gates can be efficiently implemented; in particular, sophisticated implementation methods in the context of a Hamiltonian simulation can be utilized.

### 3. Computational cost

We now consider the computational cost of preparing the ground state of the Hamiltonian  $\mathcal{H}$  using multiple steps of the approximate non-unitary operator in Sec. S1 A 2. We prepared  $K$  ancilla qubits and each of which is used for each PITE step. The input state, including ancillae qubits, is given by  $|\psi\rangle \otimes |0\rangle^{\otimes K}$ . The action of the  $K$  steps of the quantum circuit for the approximate non-unitary operator leads to

$$F_K(\mathcal{H})|\psi\rangle \otimes |0\rangle^{\otimes K} + (\text{other states}). \quad (\text{S8})$$

When measuring all the ancillae qubits as  $|0\rangle^{\otimes K}$  state, it leads to collapse from the entangled wave function to

$$|\Psi_K\rangle = \frac{1}{\sqrt{P_K}} F_K(\mathcal{H})|\psi\rangle, \quad (\text{S9})$$

where  $P_K$  is the total success probability of all the PITE steps being successful. When a initial target-qubits state is expanded as

$$|\psi\rangle = \sum_{i=1}^N c_i |\lambda_i\rangle, \quad (\text{S10})$$

the infidelity  $\delta_K$  for the  $K$  steps is calculated as

$$\delta_K = 1 - |\langle \lambda_1 | \Psi_K \rangle|^2 = 1 - \frac{1}{P_K} |c_1|^2 F_K^2(\lambda_1). \quad (\text{S11})$$

From the above relation, the total success probability is expressed as

$$P_K = \frac{1}{1 - \delta_K} |c_1|^2 F_K^2(\lambda_1). \quad (\text{S12})$$

$F_K^2(\lambda_1)$  is the  $k$ -product of  $f_k^2(\lambda_1)$ :  $F_K^2(\lambda_1) = \prod_{k=1}^K f_k^2(\lambda_1)$  and  $f_k^2(\lambda_1)$  takes a real value in the range  $[0, 1]$ . Thus, the total success probability decays exponentially as PITE step proceeds. This exponential decay can be avoided by shifting the origin of the Hamiltonian such that  $F_K^2(\lambda_1) = 1$ . In the approximate PITE, this constant energy shift can be achieved by

$$E_k = \lambda_1 - \frac{1}{\Delta\tau_k s_k} \left[ \tan^{-1} s_k - \frac{\pi}{2} (2n + 1) \right], \quad (\text{S13})$$

with an integer  $n$  for  $\lambda_i \rightarrow \lambda_i - E_k$ . Correspondingly, in the quantum circuit for the approximate PITE [Fig. S1(b)], we change the rotation angle of the  $R_z$  gate as  $2\theta_k \rightarrow 2\theta_k + 2E_k s_k \Delta\tau_k$ .

The total success probability can be expressed differently from Eq. (S12) as

$$P_K = |c_1|^2 F_K^2(\lambda_1) + \sum_{i>1} |c_i|^2 F_K^2(\lambda_i). \quad (\text{S14})$$

From Eqs. (S12) and (S14), we have

$$\frac{\delta_K}{1 - \delta_K} = \sum_{i>1} \frac{|c_i|^2 F_K^2(\lambda_i)}{|c_1|^2 F_K^2(\lambda_1)}. \quad (\text{S15})$$

The right-hand side of Eq. (S15) was evaluated in detail in Ref. [S30] where the left-hand side of Eq. (S15) is expressed as  $\tilde{\varepsilon} = \delta_K / (1 - \delta_K)$ .  $\tilde{\varepsilon}$  means an error defined as  $\tilde{\varepsilon} = \varepsilon(4 - \varepsilon) / (2 - \varepsilon)^2$  with  $\varepsilon = \|\Gamma e^{-\mathcal{H}\tau} |\psi\rangle - F_K(\mathcal{H}) |\psi\rangle\|^2$ . In conclusion, if  $\Delta\tau_k$  is chosen to vary in a linearly increasing way and the constant energy shift in Eq. (S13) is adopted, the number of steps required to achieve an infidelity  $\delta_K$  can be estimated as

$$K = \mathcal{O} \left( \ln \left( \frac{(1 - \delta_K)(1 - |c_1|^2)}{\delta_K |c_1|^2} \right) \right). \quad (\text{S16})$$

Finally, we arrive at the following equation for the computational cost of PITE presented in the main text:

$$\frac{d_{\text{CRTE}} K}{P_K} = \mathcal{O} \left( \frac{d_{\text{CRTE}} \ln \left( \frac{(1 - \delta_K)(1 - |c_1|^2)}{\delta_K |c_1|^2} \right)}{|c_1|^2} \right), \quad (\text{S17})$$

where  $d_{\text{CRTE}}$  denotes the circuit depth of the CRTE operator.

## B. Cosine propagation

Previous studies [S9, S12, S15, S48] established a quantum circuit for the non-unitary cosine function for the Hamiltonian  $\mathcal{H}$  as,

$$f_k^{(\text{cos})}(\mathcal{H}) = \cos [(\mathcal{H} - E)t_k], \quad (\text{S18})$$

which is shown in Fig. S1(c) where  $Z(\theta) = Z_\theta = |0\rangle\langle 0| + e^{i\theta}|1\rangle\langle 1|$  denotes the phase gate. Multiple operations using the cosine function decrease the weight of the states whose eigenvalues are not equal to an given energy  $E$ . Ref. [S12] uses only single CRTE gate as shown in Fig. S1(d), which also provides the cosine propagation ignoring the global phase:

$$\tilde{f}_k^{(\text{cos})}(\mathcal{H}) = \frac{1}{2} \left[ I_{2^n} + e^{-2i(\mathcal{H}-E)t_k} \right] = e^{-i(\mathcal{H}-E)t_k} \cos [(\mathcal{H} - E)t_k]. \quad (\text{S19})$$

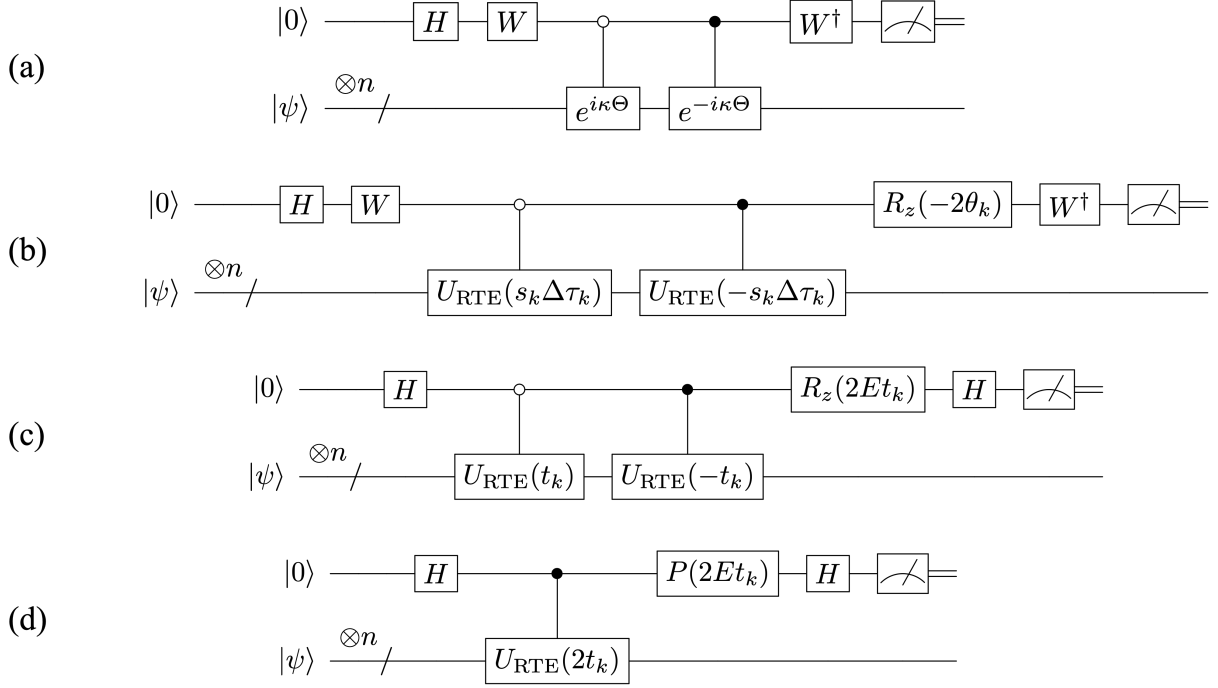


FIG. S1. (a) Quantum circuit  $\mathcal{C}_M$  for the probabilistic operation of a non-unitary  $M$  that acts on an input  $n$ -qubit state  $|\psi\rangle$ . (b) Quantum circuit  $\mathcal{C}_{\text{PITE}}^{(1)}$  is equivalent to  $\mathcal{C}_{\text{PITE}}$  in the first order of  $\Delta\tau$ . (c) Quantum circuit  $\mathcal{C}_{\text{cos}}$  for cosine propagation. (d) Equivalent quantum circuit to  $\mathcal{C}_{\text{cos}}$  realized by a single CRTE gate by ignoring global phase.  $H$  and  $Z(\theta)$  represent Hadamard and phase gates, respectively.

## S2. QUANTUM PHASE ESTIMATION BASED ON QUANTUM FOURIER TRANSFORMATION

In this section, we review the gate complexity for preparing the ground state with the quantum phase estimation (QPE) for a known ground energy, as presented in Proposition 3 in Ref. [S9]. The quantum circuit for QPE based on the quantum Fourier transformation (QFT) [S51] changes the initial target qubits state,  $|\psi\rangle = \sum_{i=1}^N c_i |\lambda_i\rangle$  and  $K$  ancillae qubits to

$$|\psi\rangle \otimes |0\rangle^{\otimes K} \rightarrow \sum_{k=0}^{T-1} \underbrace{\sum_{i=1}^N c_i \alpha_{ik} |\lambda_i\rangle \otimes |k\rangle}_{\equiv |\Phi_k\rangle}, \quad (\text{S20})$$

where

$$\alpha_{ik} \equiv \frac{1}{T} \sum_{\tau=0}^{T-1} e^{2\pi i \tau (\lambda_i t_0 - k) / T} = \frac{1}{T} \left( \frac{1 - e^{2\pi i (T\lambda_i t_0 - k)}}{1 - e^{2\pi i (\lambda_i t_0 - k / T)}} \right), \quad (\text{S21})$$

and  $T \equiv 2^K$ .  $t_0$  is a scaling parameter to enlarge or shrink the range of searching eigenvalues introduced for precise estimation. The post-selecting state with respect to eigenvalue  $k$  in the binary representation is given by

$$|\Psi_{\text{QFT}}\rangle = \frac{1}{\sqrt{P_k}} \sum_{i=1}^N c_i \alpha_{ik} |\lambda_i\rangle, \quad (\text{S22})$$

where the state is normalized with the success probability expressed as

$$P_k = \sum_{i=1}^N |c_i|^2 |\alpha_{ik}|^2. \quad (\text{S23})$$

The infidelity of  $|\Psi_{\text{QFT}}\rangle$  is calculated as

$$\delta = 1 - |\langle \lambda_1 | \Psi_{\text{QFT}} \rangle|^2 = \frac{\sum_{i>1} |c_i|^2 |\alpha_{ik}|^2}{\sum_{i=1}^N |c_i|^2 |\alpha_{ik}|^2}. \quad (\text{S24})$$

The success probability is rewritten with the infidelity as

$$P_k = \frac{1}{1 - \delta} |c_1|^2 |\alpha_{1k}|^2. \quad (\text{S25})$$

For deriving the scaling of  $K$  with respect to  $\delta$ , we investigate the inequality for  $\alpha_{ik}$ . By using  $|1 - e^{i\theta}| \geq 2$  for  $\theta \in \mathbb{R}$ , we have

$$|\alpha_{ik}| \leq \frac{2}{T|1 - e^{2\pi i(\lambda_i t_0 - k/T)}|}. \quad (\text{S26})$$

For  $\theta \in [-\pi, \pi]$ , we know

$$\frac{2}{\pi} |\theta| \leq |1 - e^{i\theta}| \leq |\theta|, \quad (\text{S27})$$

which leads to relations [S51]

$$\frac{1}{\pi T \Delta} \leq |\alpha_{ik}| \leq \frac{1}{2T\Delta}, \quad (\text{S28})$$

where  $\Delta \equiv |\lambda_i t_0 - k/T|$ . In addition, when  $k$  satisfies  $\Delta = |\lambda_i t_0 - k/T| < 1/2T$ , we have [S9]

$$\frac{2}{\pi} \leq |\alpha_{ik}|. \quad (\text{S29})$$

Using two inequalities (S28) and (S29), the infidelity  $\delta$  in Eq. (S24) is bounded as

$$\delta \leq \frac{\sum_{i>1} |c_i|^2 |\alpha_{ik}|^2}{|c_1|^2 |\alpha_{1k}|^2} \leq \left( \frac{\pi}{4|c_1|T\Delta} \right)^2 (1 - |c_1|^2) \leq \left( \frac{\pi}{4|c_1|T\Delta} \right)^2. \quad (\text{S30})$$

To achieve infidelity being  $\delta$ , it is sufficient to take  $K$  as

$$2^K = \mathcal{O} \left( \frac{1}{\sqrt{\delta} |c_1| \Delta} \right). \quad (\text{S31})$$

The number of queries of CRTE is scales as  $\mathcal{O}(2^K)$ . Because the controlling unitary gate of the QPE is a CRTE gate in this case, we need to perform a Hamiltonian simulation in real time multiplied by  $\mathcal{O}(2^K)$ . As a simple case, we can implement the CRTE gate by dividing such a long real-time into  $\mathcal{O}(2^K)$  parts. The computational cost of QFT is relatively small compared with the CRTE sequences; thus, the depth of the quantum circuit for QPE is expressed as

$$d_{\text{QPE}} = \mathcal{O}(2^K d_{\text{CRTE}}) = \mathcal{O} \left( \frac{d_{\text{CRTE}}}{\sqrt{\delta} |c_1| \Delta} \right). \quad (\text{S32})$$

By taking into account for the success probability in Eq. (S25), the computational cost for QPE is given by

$$\frac{d_{\text{QPE}}}{P_k} = \mathcal{O} \left( \frac{d_{\text{CRTE}}(1 - \delta)}{\sqrt{\delta} |c_1|^3 \Delta} \right), \quad (\text{S33})$$

where we assumed  $|\alpha_{1k}| = \mathcal{O}(1)$ . Importantly, the computational cost of the QPE for providing the ground state energy is scaled as  $\mathcal{O}(1/|c_1|^3)$ . Note that suitable amplitude amplification technique reduces the computational cost to [S9]

$$\frac{d_{\text{QPE}}}{P_k} = \mathcal{O} \left( \frac{d_{\text{CRTE}}(1 - \delta)}{\sqrt{\delta} |c_1|^2 \Delta} \right), \quad (\text{S34})$$

leading to the scaling of  $\mathcal{O}(1/|c_1|^2)$ .

### S3. QUANTUM CIRCUIT FOR CONTROLLED-REAL-TIME EVOLUTION

#### A. Lie-Trotter-Suzuki decomposition

The Hamiltonian for a closed one dimensional Heisenberg model in the main text is presented as

$$\mathcal{H} = \sum_{\langle j, k \rangle} \vec{\sigma}_j \cdot \vec{\sigma}_k + \sum_j h_j \sigma_j^z, \quad (\text{S35})$$

where  $\vec{\sigma}_j = (\sigma_j^x, \sigma_j^y, \sigma_j^z)$  and  $\langle j, k \rangle$  represent the combination of the nearest neighbors of the closed one-dimensional chain.  $h_j$  represents the strength of the magnetic field, which was randomly chosen from a uniform distribution as  $h_j \in [-1, 1]$ . The Hamiltonian is divided into two groups in an even-odd manner [S22, S23]:

$$\mathcal{H} = \mathcal{H}_1 + \mathcal{H}_2, \quad (\text{S36})$$

where

$$\begin{aligned} \mathcal{H}_1 &= \sum_{j=1}^{\lfloor n/2 \rfloor} (\vec{\sigma}_{2j-1} \cdot \vec{\sigma}_{2j} + h_{2j-1} \sigma_{2j-1}^z) \\ \mathcal{H}_2 &= \sum_{j=1}^{\lceil n/2 \rceil - 1} (\vec{\sigma}_{2j} \cdot \vec{\sigma}_{2j+1} + h_{2j} \sigma_{2j}^z). \end{aligned} \quad (\text{S37})$$

Note that although all the summands in the sub-Hamiltonian commute with each other, but  $\mathcal{H}_1$  and  $\mathcal{H}_2$  do not:  $[\mathcal{H}_1, \mathcal{H}_2] \neq 0$ . Namely, RTE for the sub-Hamiltonian is exactly decomposed as

$$e^{i\mathcal{H}_1 t} = \prod_{j=1}^{\lfloor n/2 \rfloor} U_{2j-1, 2j}, \quad e^{i\mathcal{H}_2 t} = \prod_{j=1}^{\lceil n/2 \rceil - 1} U_{2j, 2j+1}, \quad (\text{S38})$$

where  $U_{ij}$  is the two-qubit gate unitary operation.

$$U_{ij} = \exp [it (\vec{\sigma}_{2j} \cdot \vec{\sigma}_{2j+1} + h_{2j} \sigma_{2j}^z)]. \quad (\text{S39})$$

The implementation of RTE for the total Hamiltonian  $\mathcal{H} = \mathcal{H}_1 + \mathcal{H}_2$  is realized using the Lie-Trotter-Suzuki formula [S45]:

$$\mathcal{S}_1(t) = e^{itH_1} e^{itH_2} + \mathcal{O}(t^2) \quad (\text{S40})$$

$$\mathcal{S}_2(t) = e^{i(t/2)H_1} e^{itH_2} e^{i(t/2)H_1} + \mathcal{O}(t^3) \quad (\text{S41})$$

$$\mathcal{S}_{2k}(t) = \mathcal{S}_{2k-2}^2(u_k t) \mathcal{S}_{2k-2}((1-4u_k)t) \mathcal{S}_{2k-2}^2(u_k t) + \mathcal{O}(t^{2k+1}), \quad (\text{S42})$$

where

$$u_k \equiv \frac{1}{4 - 4^{\frac{1}{2k-1}}}. \quad (\text{S43})$$

The even-order Trotter decomposition  $\mathcal{S}_{2k}(t)$  is recursively written using the previous even operator  $\mathcal{S}_{2k-2}(t)$ . The circuit depth for  $\mathcal{S}_{2k}(t)$  is expressed as  $d_{\mathcal{S}_{2k}} = 5^{k-1} d_{\mathcal{S}_2}$ .

Consider simulating RTE of an operator  $\mathcal{H} = \sum_{\gamma=1}^{\Gamma} \mathcal{H}_{\gamma}$  consisting of anti-Hermitian operator  $\mathcal{H}_{\gamma}$ . For long-time simulation, the simulation time  $t \geq 0$  is divided into  $r$  steps, and  $p$ th-order Trotter-Suzuki decomposition is applied. Achieving accuracy

$$\left\| \mathcal{S}_p^r \left( \frac{t}{r} \right) - e^{t\mathcal{H}} \right\| = \mathcal{O}(\epsilon), \quad (\text{S44})$$

is realized by using Trotter number  $r$  [S23]:

$$r = \mathcal{O} \left( \frac{\tilde{\alpha}_{\text{comm}}^{1/p} t^{1+1/p}}{\epsilon} \right), \quad (\text{S45})$$

where  $\tilde{\alpha}_{\text{comm}}$  is the norm of commutator defined as

$$\tilde{\alpha}_{\text{comm}} \equiv \|[H_{\gamma_{p+1}}, \dots, [H_{\gamma_2}, H_{\gamma_1}] \dots]\| . \quad (\text{S46})$$

When  $p$  is chosen to be sufficiently large, the Trotter number  $r$  scales as

$$r = \mathcal{O} \left( \frac{\tilde{\alpha}_{\text{comm}}^{o(1)} t^{1+o(1)}}{\epsilon} \right) . \quad (\text{S47})$$

## B. Quantum circuit for controlled two-qubit unitary

In Sec. S3 A, the RTE for the Heisenberg Hamiltonian is divided into the product of two-qubit unitary. PITE and QPE comprise the CRTE operations. This section presents the quantum circuit for a controlled two-qubit unitary. First, any two-qubit unitary can be decomposed as

$$U_{ij} = e^{i\theta_g} (V_i \otimes V_j) R_d(\vec{\theta}) (W_i \otimes W_j) , \quad (\text{S48})$$

where  $R_d(\vec{\theta})$  is a diagonal two-qubit unitary:

$$R_d(\vec{\theta}) = e^{i(\theta_x \sigma_i^x \otimes \sigma_j^x + \theta_y \sigma_i^y \otimes \sigma_j^y + \theta_z \sigma_i^z \otimes \sigma_j^z)} . \quad (\text{S49})$$

The rotation angles  $\vec{\theta} = (\theta_x, \theta_y, \theta_z)$ , global phase  $\theta_g$ , and single-qubit gates  $\{V_i, V_j, W_i, W_j\}$  are determined using Cartan's KAK decomposition [S52], which is implemented in Cirq [S53]. The diagonal two-qubit unitary  $R_d(\vec{\theta})$  is implemented using three CNOT gates, ignoring the global phase, which is denoted by  $C_d(\vec{\theta})$ .

$$R_d(\vec{\theta}) = e^{i\pi/4} C_d(-2\vec{\theta}) . \quad (\text{S50})$$

The quantum circuit of  $C_d(\vec{\theta})$  is shown in Fig. S2.

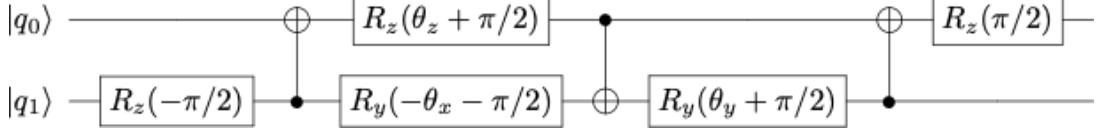


FIG. S2. Quantum circuit for the diagonal two-qubit rotation gate ignores the global phase  $C_d(\vec{\theta}) = e^{-i\pi/4} R_d(-\vec{\theta}/2)$ .

This implementation scheme is the most efficient method for any two-qubit unitary and does not require any approximation as Trotter decomposition; thus, we extend the circuit to the controlled two-qubit unitary. The controlled operation of  $U_{ij}$  is realized by enabling rotation angles  $\{\theta_x, \theta_y, \theta_z\}$  when the ancilla qubit is  $|1\rangle$  state. In addition, the single-qubit gates  $V_i$  and  $W_i$  do not cancel each other out,  $V_i W_i \neq I_2$ , in general. Thus, these single-qubit gates should be applied depending on the state of the control qubit.  $W_i$  gate is rewritten as  $W_i = W_i V_i V_i^\dagger$  to reduce the CNOT gates. Then, the  $V_i^\dagger$  gate is implemented as a single-qubit gate, and  $W_i V_i$  gate is implemented as a controlled unitary gate. Therefore, the quantum circuit for the controlled unitary  $U_{ij}$  is shown in Fig. S3. The following equations demonstrate that the quantum circuit, shown in Fig. S3 is controlled  $U_{ij}$  operation.

$$\begin{aligned} & Z_{\theta_g} \otimes I_4 \left( |0\rangle\langle 0| \otimes (V_i \otimes V_j) C_d(\vec{\theta} = \vec{0}) (V_i^\dagger \otimes V_j^\dagger) + |1\rangle\langle 1| \otimes (V_i \otimes V_j) C_d(-2\vec{\theta}) (W_i \otimes W_j) \right) \\ &= e^{-i\pi/4} Z_{\theta_g} \otimes I_4 \left( |0\rangle\langle 0| \otimes I_4 + |1\rangle\langle 1| \otimes (V_i \otimes V_j) R_d(\vec{\theta}) (W_i \otimes W_j) \right) \\ &= e^{-i\pi/4} Z_{\theta_g} \otimes I_4 \left( |0\rangle\langle 0| \otimes I_4 + |1\rangle\langle 1| \otimes e^{-i\theta_g} U_{ij} \right) \\ &= e^{-i\pi/4} (|0\rangle\langle 0| \otimes I_4 + |1\rangle\langle 1| \otimes U_{ij}) . \end{aligned} \quad (\text{S51})$$

Because the controlled unitary gate is implemented using two CNOT gates [S51], the controlled unitary  $U_{ij}$  requires 13 CNOT gates.

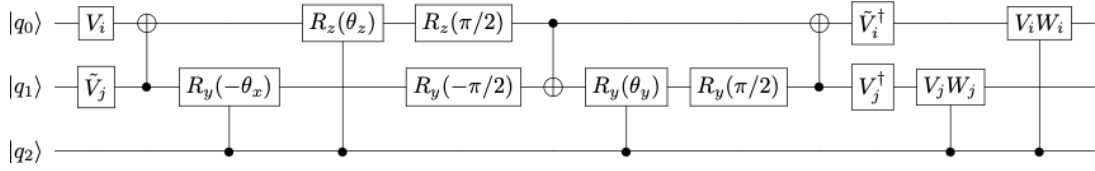


FIG. S3. Quantum circuit for controlled-two-qubit unitary gate using KAK decomposition, ignoring the global phase. The lowest qubit is the control qubit and the other qubits are the target qubits.  $\tilde{V}_j = R_z(-\pi/2)V_j$  and  $\tilde{V}_i^\dagger = V_i^\dagger R_z(\pi/2)$  are used in this figure.

#### S4. DETAILS OF NUMERICAL RESULTS

##### A. Setup

This section presents additional numerical results to provide deep insights into the PITE, multi-step PITE, and QPE. We use same computational model in main text, which is the Heisenberg model expressed as

$$\mathcal{H} = \sum_{\langle j, k \rangle} \vec{\sigma}_j \cdot \vec{\sigma}_k + \sum_j h_j \sigma_j^z, \quad (\text{S52})$$

where  $\vec{\sigma}_j = (\sigma_j^x, \sigma_j^y, \sigma_j^z)$  and  $\langle j, k \rangle$  represent the combination of the nearest neighbors of the closed one-dimensional chain.  $h_j$  represents the strength of the magnetic field, which was randomly chosen from a uniform distribution as  $h_j \in [-1, 1]$ .

As discussed in our previous study [S30], an appropriate constant energy shift avoids the exponential decay of the total success probability when increasing the PITE step. This constant energy shift is adopted in the numerical simulation. In addition, the imaginary-time step size can be changed step by step, here we adopted

$$\Delta\tau_k = (1 - e^{-(k-1)/\kappa})(\Delta\tau_{\max} - \Delta\tau_{\min}) + \Delta\tau_{\min}, \quad (\text{S53})$$

where  $\kappa$  is introduced to control the speed of the change. The larger  $\kappa$  leads to rapid change  $\Delta\tau_k$  from  $\Delta\tau_{\min}$  to  $\Delta\tau_{\max}$ , and smaller  $\kappa$  is opposite. The behavior of the infidelity of PITE by changing the parameters  $\Delta\tau_{\min}$ ,  $\Delta\tau_{\max}$ ,  $\bar{\kappa}$  was also studied in Ref. [S30]. The study concluded that mixing a certain level of nonlinearity into linear scheduling is a good approach for suppressing infidelity and accelerating the computational time to prepare the ground state. Based on the previous reports, we use  $\Delta\tau_{\min} = \pi/(2s\Delta\tau_N)$ ,  $\Delta\tau_{\max} = \pi/(s\Delta\tau_2)$ , and  $\bar{\kappa} \equiv \kappa/K = 1$ .

##### B. Dependence on the order of Trotter decomposition for CRTE

We performed QPE and PITE by changing the number of steps  $K$  and plotted the total success probability  $P_K$  and infidelity defined as  $\delta \equiv 1 - \mathcal{F}$  with fidelity  $\mathcal{F}$  in Fig. S4. The initial state is prepared as a uniform probability weight for each eigenstate,  $|c_i| = 1/\sqrt{N}$ . The number of steps for QPE corresponds to the number of ancillary qubits used to determine the accuracy of the eigenvalue in the binary representation loaded in the ancilla qubit. The implementation of the CRTE gates in QPE and PITE was employed by Trotter-Suzuki decomposition, and we changed the order of Trotter-Suzuki decomposition to first-, second-, and fourth-order. As the QPE still has a numerical error for the CRTE gates, we further divide the time of the RTE operator by  $r = 4$ . The scaling parameter  $t_0$  of the QPE to enlarge or shrink the searching range of the eigenvalues for precise estimation is adopted as  $t_0 = 2^{K-N_C}$ , where  $N_C = \lfloor \log_2(\lambda_N - \lambda_1) \rfloor$ . It should be noted that  $\{\Delta\tau_k\}$  of PITE was calculated using Eq. (S53) with  $\Delta\tau_{\max}$  and  $\Delta\tau_{\min}$  are fixed and the number of steps  $K$ . In other words,  $\{\Delta\tau_k\}$  was calculated for each plot point.

First, we consider the total success probability  $P_K$  in Figs. S4(a, b). As discussed in the main text, the total success probability is given by  $P_K = |c_1|^2/(1 - \delta)$ , which is depicted by dotted black lines with  $\delta = 0$ . The QPE with the fourth-order Trotter decomposition shows good agreement with  $P_K = |c_1|^2$  line. In contrast, the first- and second-order cases deviated from the ideal value, and the amount of deviation was prominent in a large number of steps. This deviation is considered to be the cause of the error due to insufficient Trotter-Suzuki decomposition for non-commutator terms. The total success probabilities for PITE converge to the ideal value in small steps for every order of Trotter-Suzuki decomposition.

From the results in Figure S4(c, d), we can see that the fourth-order Trotter decomposition presents good accuracy, coinciding with the exact implementation of the CRTE operator for QPE and PITE. The first- and second-order

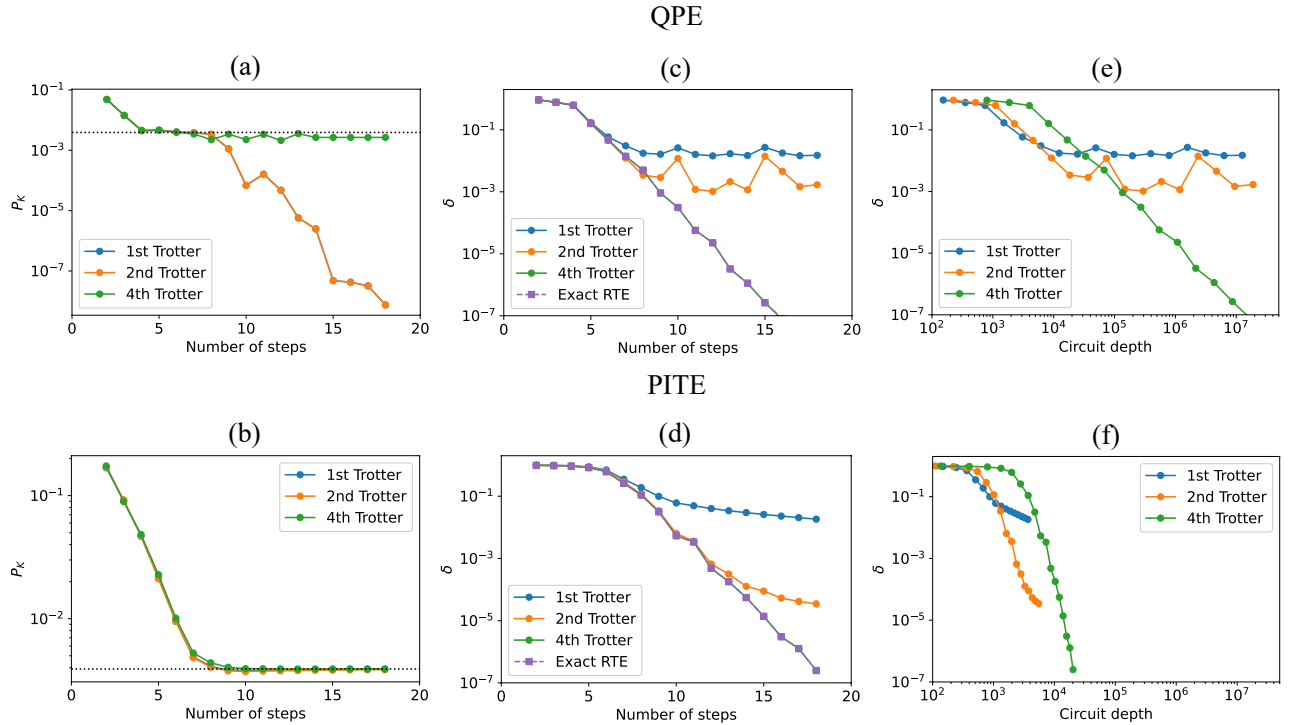


FIG. S4. The numerical simulation for ground-state preparation was performed using the Heisenberg model in a one-dimensional chain with eight spins. Total success probability  $P_K$  according to the number of steps for QPE (a) and PITE (b). The dotted black line represents the probability weight of the ground state, which is a theoretically estimated value (see main text). Infidelity  $\delta \equiv 1 - \mathcal{F}$  with fidelity  $\mathcal{F}$  was plotted by changing the number of steps for QPE (c) and PITE (d). The infidelity as a function of the circuit depth for QPE (e) and PITE (f) is presented. The CRTE gates are implemented using first- (blue line), second- (orange line), and fourth-order (green line) Trotter-Suzuki decomposition. The exact implementation of the CRTE gate is indicated by purple lines.

Trotter decompositions deviate from the exact RTE result and saturate the error in a certain infidelity. PITE exhibits the same behavior; however, the amount of error decreases as the order of the Trotter decomposition increases. We found that PITE is robust to errors from Trotter-Suzuki decomposition.

Finally, we estimated the circuit depth for the QPE and PITE and plotted them in Figs. S4(e, f). For simplicity, the computational cost of the quantum circuit for the initial state was ignored. We implemented the CRTE gates using Qiskit [S44] and calculated the circuit depth for one CRTE gate,  $d_{\text{CRTE}}$ . We then estimated the circuit depth from the depth of the CRTE gate and the number of queries to the CRTE gates. The circuit depth for QPE is estimated as

$$d_{\text{QPE}} = 1 + (2^K - 1)r d_{\text{CRTE}} + d_{\text{QFT}}^{(K)} \quad (\text{S54})$$

where  $d_{\text{QFT}}^{(K)}$  represents the circuit depth of QFT with  $K$  qubits. In Fig. S4(e), QPE presents the Heisenberg scaling, where the circuit depth linearly increases as the infidelity decreases. In contrast, the circuit depth for the PITE logarithmically increased as infidelity decreased. In other words, the analytical estimation of the main text was confirmed. This exponential improvement over QPE arises from the linear increase in the imaginary time-step size  $\Delta\tau_k$ . Actually, we use exponential scheduling; however, the increasing speed of  $\Delta\tau_k$  is adjusted to be linear by parameter  $\bar{\kappa}$ . The circuit depth for PITE is calculated as

$$d_{\text{PITE}} = 4 + K(K - 1)d_{\text{CRTE}}. \quad (\text{S55})$$

Accordingly, the number of queries to CRTE exhibits a linear increase in PITE, leading to an exponential advantage over QPE with respect to infidelity.

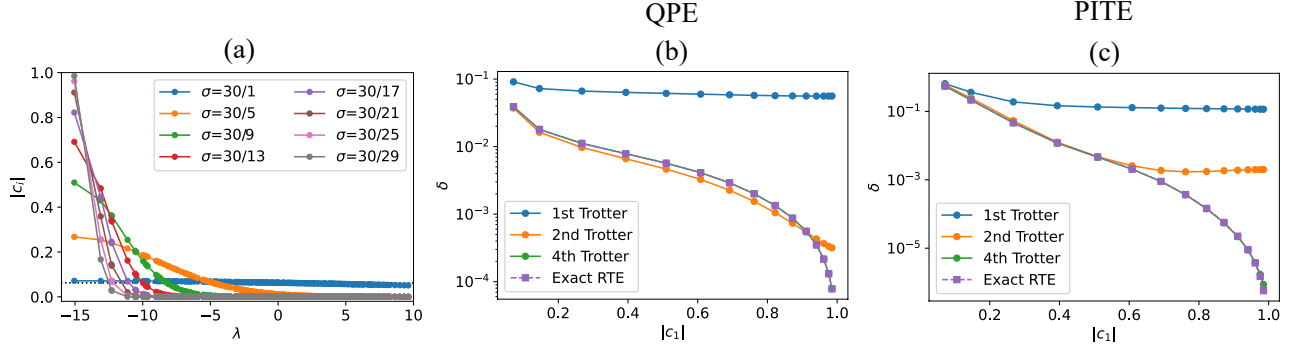


FIG. S5. Numerical simulation for ground state preparation was performed using the Heisenberg model in a one-dimensional chain with eight spins. (a) Probability weights of the initial state as a function of eigenvalues that follow a Gaussian distribution given by Eq. (S56). Variances  $\sigma$  are plotted in different colors. The dotted black line represents the uniform probability weight  $|c_i| = 1/\sqrt{N}$ . The infidelity according to the ground-state weight  $|c_1|$  is plotted for (b) QPE and (c) PITE. The number of steps was fixed at  $K = 6$ .

### C. Dependence on the probability weight of the ground state in the initial state

The first numerical simulation was performed using a superposition state for each eigenstate, with a uniform probability weight. However, this scenario is unrealistic. Numerous proposals and applications have been proposed for the approximate calculation of the ground state using a classical computer. For example, density functional theory (DFT) [S54, S55] is widely used in materials science. In addition, the coupled cluster method starts from the initial state obtained by the Hartree-Fock (HF) calculation [S56, S57], and the use of DFT or HF states as an initial state is an adequate possible scenario.

A good initial state leads to a high total success probability in QPE and PITE. Thus, we calculated the errors for the QPE and PITE by changing the probability weight of the initial state. As an example, the initial state weight was obtained from a Gaussian distribution.

$$c_i \propto \exp\left(-\frac{(\lambda_i - \lambda_1)^2}{2\sigma^2}\right), \quad (\text{S56})$$

where  $\sigma$  denotes the variance. The initial state probability weights used in this study are shown in Fig. S5(a). The mean of  $\lambda_1$  is concentrated in the probability weight of the ground state by decreasing  $\sigma$ . A uniform probability weight corresponds to a large value limit of  $\sigma$ . In the numerical simulation, we used  $\sigma = 30/i$  for  $i = 1, 2, \dots, 29$ .

The infidelity for the QPE and PITE according to  $|c_1|$  is presented in Figs S5(b, c), respectively. The number of steps is fixed at  $K = 6$ . In both methods, infidelity decreases as  $|c_1|$  increases. An increase in the probability weight of the ground state corresponds to a decrease in infidelity. In addition, reducing the probability weight of the high-energy states decreases the effect of the noncommutator in the Trotter-Suzuki approximation.

### D. Details of estimation of circuit depth for multi-step PITE

The entire quantum circuit of multi-step PITE consists of the first acting PITE and  $m^*$  iterations of the amplitude amplification operator. The circuit depth of multi-step PITE is given by

$$d_{\text{PITE+AA}} = m^* \left( 2d_{\text{PITE}} + d_{S_0}^{(K)} + d_{S_0}^{(n+K)} + 2d_{U_{\text{ref}}} \right) + d_{\text{PITE}}, \quad (\text{S57})$$

where

$$m^* = \left\lfloor \frac{(2n+1)\pi}{4 \sin^{-1} \sqrt{P_K}} \right\rfloor, \quad (\text{S58})$$

where  $n$  is an integer.  $d_{\text{PITE}}$  represents the circuit depth of the approximated PITE for  $K$  steps.  $d_{S_0}^{(n)}$  represents the circuit depth for zero reflections of  $n$  qubits.  $d_{U_{\text{ref}}}$  represents the circuit depth for quantum circuit  $U_{\text{ref}}$ , which creates the initial state  $|\psi\rangle$  from  $|0\rangle^{\otimes n}$  state.

Here, we are particularly interested in the following question: When is adopting QAA more beneficial than adopting PITEs without QAA? If  $P_K$  is sufficiently large, adopting QAA is inefficient in terms of computational cost. The total success probability  $P_K$  for  $m^*$  repetition is expressed as

$$\sin\left(\frac{\pi}{4(m^* + 1)}\right) < \sqrt{P_K} \leq \sin\left(\frac{\pi}{4m^*}\right), \quad (\text{S59})$$

where the upper bound of  $\sqrt{P_K}$  is one when  $m^* = 0$ . Tuning the PITE parameter  $\gamma$  succeeds the deterministic operation of the ITE operator by increasing the QAA repetition to  $m^* + 1$ . If  $1/2 < P_K \leq 1$  where  $m^* = 1$ , then it is easy to show that  $d_{\text{PITE+AA}}$  is always larger than the computational cost of the PITE. For the other cases, we approximate  $m^*$  as  $m^* \approx \pi/(4\sqrt{P_K})$  to derive a relationship such that the adoption of QAA is beneficial.

$$d_{\text{PITE}} \geq \frac{\pi|c_1|}{4(1 - |c_1|^2)} \left( d_{S_0}^{(K)} + d_{S_0}^{(n+K)} + 2d_{U_{\text{ref}}} \right). \quad (\text{S60})$$

This relation implies that adopting QAA is useful when the implementation cost for zero reflection is lower than that for PITE or when the probability weight of the ground state is sufficiently small.